
Diffusion Denoised Smoothing for Certified and Adversarial Robust Out-Of-Distribution Detection

Nicola Franco¹ Daniel Korth¹ Jeanette Miriam Lorenz¹ Karsten Roscher¹ Stephan Günnemann²

Abstract

As the use of machine learning continues to expand, the importance of ensuring its safety cannot be overstated. A key concern in this regard is the ability to identify whether a given sample is from the training distribution, or is an "Out-Of-Distribution" (OOD) sample. In addition, adversaries can manipulate OOD samples in ways that lead a classifier to make a confident prediction. In this study, we present a novel approach for certifying the robustness of OOD detection within a ℓ_2 -norm around the input, regardless of network architecture and without the need for specific components or additional training. Further, we improve current techniques for detecting adversarial attacks on OOD samples, while providing high levels of certified and adversarial robustness on in-distribution samples. The average of all OOD detection metrics on CIFAR10/100 shows an increase of $\sim 13\%/5\%$ relative to previous approaches.

1. Introduction

Although recent advances in Machine Learning (ML) demonstrate its validity in a wide range of applications, its use in safety-critical conditions remains challenging. Since the appearance of unexpected low robustness to natural (Hendrycks & Dietterich, 2018; Engstrom et al., 2019) and adversarial (Biggio et al., 2013; Szegedy et al., 2014) perturbations to the input data, several types of defenses have been proposed along the years. Two main branches of defenses exist: *empirical* (Goodfellow et al., 2015; Carlini & Wagner, 2017; Madry et al., 2018) and *certified* (Katz et al., 2017; Zhang et al., 2018; Wong & Kolter, 2018; Cohen et al., 2019), which aim at *improving* or *assuring* the robustness of the prediction in the vicinity of the input, respectively. For the sake of clarity, in this paper we refer to

empirical robustness as *adversarial* robustness.

Certified defenses might give the inaccurate impression that robustness makes ML systems ready for deployment in safety-critical applications. Unfortunately, the certified robustness of a model does not necessarily mean that its prediction is always accurate (Franco et al., 2023). Further issues lie also beyond robustness, because deep-learning-based models have numerous problems, including the lack of guarantees for Out-Of-Distribution (OOD) data, the lack of fairness, or the lack of explainability (Paley et al., 2022).

In the field of OOD detection, several studies emphasize the importance of ensuring low confidence in the presence of OOD data (Hein et al., 2019; Bitterwolf et al., 2020; Meinke et al., 2022). These methods incorporate both certified defenses and standard OOD detection techniques (Hendrycks & Gimpel, 2017; Hendrycks et al., 2019; Du et al., 2021; Wei et al., 2022). Similar to In-Distribution (ID), robustness for OOD detection can be separated into two types: *adversarial* and *certified*. Adversarial attacks heuristically maximize the confidence for OOD samples within a ℓ_p -norm around the input. If the model can maintain low confidence under these attacks, then it is adversarially robust. In contrast, certified robustness provides a formal statement of an upper bound for the maximum confidence within the same ℓ_p -norm.

It is widely recognized that increasing robustness often comes at the expense of reduced accuracy (Jovanovic et al., 2021). This applies to robust OOD detection as well. Recently, a new approach was suggested to improve robustness in the ℓ_∞ -norm by adding a certified binary discriminator, while maintaining high top-1 accuracy on ID data (Meinke et al., 2022). However, this method does not provide adequate adversarial and certified robustness for ID data and its results for certified robustness on OOD samples are not yet usable in practice, suggesting the need for new approaches.

In this study, we propose a novel technique for certifying OOD detection within the ℓ_2 -norm of the input sample, without requiring the use of binary discriminators or specific training. This enables us to establish a guaranteed upper bound on the classifier's confidence within a defined region surrounding the input. Unlike before, certified robust OOD detection can now be computed for standard OOD detec-

¹Fraunhofer Institute for Cognitive Systems IKS, Munich, Germany ²Dept. of Computer Science & Munich Data Science Institute, Technical Univ. of Munich, Germany. Correspondence to: Nicola Franco <nicola.franco@iks.fraunhofer.de>.

Table 1: Comparison between this work and previous methods in terms of ID and OOD robustness properties. In this case, the \checkmark indicates that property was provided in the work. While (\checkmark) indicates that the property is actually lower than expected.

Methods	In-Distribution (ID) Accuracy			Out-Of-Distribution (OOD) Detection				
	Clean	Adversarial ℓ_∞	Certified ℓ_2	Clean	Adversarial ℓ_∞	Certified ℓ_∞	ℓ_2	Asymptotic underconfidence
- Standard								
OE (Hendrycks et al., 2019)	\checkmark			\checkmark				
VOS (Du et al., 2021)	\checkmark			\checkmark				
LogitNorm (Wei et al., 2022)	\checkmark			\checkmark				
- Adversarial								
ACET (Hein et al., 2019)	(\checkmark)	\checkmark		\checkmark	(\checkmark)			
ATOM (Chen et al., 2021)	(\checkmark)			\checkmark	(\checkmark)			
- Guaranteed								
GOOD (Bitterwolf et al., 2020)					\checkmark	\checkmark		\checkmark
ProoD (Meinke et al., 2022)	\checkmark			\checkmark	\checkmark	\checkmark		\checkmark
DISTRO (Our)	\checkmark	\checkmark	\checkmark	\checkmark	\checkmark	\checkmark	\checkmark	\checkmark

tion approaches. Additionally, we enhance and build upon the method of Meinke et al. (2022). We incorporate a diffusion denoiser (Nichol & Dhariwal, 2021; Carlini et al., 2023), which recovers the perturbed images and returns high quality denoised inputs. This leads to better levels of both adversarial and certified robustness for ID and OOD data.

In summary, our contributions are:

- A novel technique to robustly certify the confidence of any classifier within an ℓ_2 -norm on OOD data. We utilize the local Lipschitz continuity obtained through smoothing the classifier. This yields a certified upper bound on the confidence. This method can be applied to any architecture and does not require additional components, even though it has higher computational costs compared to previous approaches.
- A method named DISTRO: **D**iffusion denoised **S**moother for **R**obust **O**OD detection. This method incorporates a diffusion denoiser model to improve the detection of adversarial and certified OOD samples, while providing high adversarial and certified accuracy for ID data.

2. Related Work

This work and previous methods are compared in Table 1.

Standard OOD Detection. Standard OOD detection is the process of identifying inputs that do not conform to the training distribution and therefore the model should abstain from making a prediction. Hendrycks & Gimpel (2017) introduced the Maximum Softmax Probability (MSP) as a baseline method for OOD detection. Assuming that ID samples should have a higher softmax probability (or confidence in the prediction) than OOD samples, a threshold is determined to distinguish between ID and OOD samples.

Outlier Exposure (OE) (Hendrycks et al., 2019) is a popular training technique. The basic idea is to train a model to distinguish between ID and OOD samples by exposing it to a large number of OOD samples during training. Afterwards, the model can be evaluated on new, unseen OOD samples. Two recent approaches are VOS (Du et al., 2021) and LogitNorm (Wei et al., 2022). Virtual Outlier Synthesis (VOS) is an original framework for detecting OOD by adaptively synthesizing virtual outliers during training. In contrast, LogitNorm assumes that the logit (pre-softmax) vector’s norm increases during training, leading to overconfident predictions. Therefore, it normalizes the logit vector by the ℓ_2 -norm to reduce this increase. Additionally, thresholding the normalized logit vector can be used as a simple and effective test to detect OOD samples.

Adversarial OOD Detection. Other lines of research, such as Hein et al. (2019); Meinke & Hein (2020); Chen et al. (2021), focus on providing low confidence for OOD data when perturbed with adversarial noise. The authors of Hein et al. (2019) show that ReLU networks can have arbitrarily high confidence for data that is *far enough* from the training distribution. They also propose an adversarial training method to enforce low confidence on OOD data, but at the cost of decreased ID accuracy. ATOM (Chen et al., 2021) addresses this issue by using outlier mining techniques to automatically select a diverse set of OOD samples from a large pool of potential OOD samples.

Guaranteed OOD Detection. Recent studies like Bitterwolf et al. (2020); Meinke et al. (2022) bring forth ℓ_∞ -norm certified robustness for OOD data with a simple but effective method: Interval Bound Propagation (IBP) (Mirman et al., 2018; Gowal et al., 2018). First, Bitterwolf et al. (2020) proposed a training approach to derive a provable upper bound on the maximum confidence of the network in an ℓ_∞ -norm of ϵ around a given sample using IBP. Although this method leads to classifiers with pointwise certified robustness even

for near-OOD samples, IBP can produce loose bounds that result in a drop in network accuracy (Jovanovic et al., 2021). Secondly, to overcome this problem, ProoD (Meinke et al., 2022) combines a certified binary discriminator, to provide adversarial and certified robustness on OOD data, with an OE model which preserves high clean accuracy. Although they achieve state-of-the-art performance in different OOD metrics and test distributions, the results are not yet useful in practice as most are still below 60%. Other downsides of this approach are: (i) it is not robust to adversarial ID attacks and has low certified ID accuracy, (ii) it does require external datasets, which are not only hard to obtain and filter, but also the generalization from a single OOD dataset to the entire OOD space is often not given, and (iii) training with IBP hurts the performance of larger discriminator models, making the method less prone to scale.

3. Background

We define a *hard* classifier as a function $f : \mathbb{R}^d \rightarrow \mathcal{Y}$ which maps input samples $x \in \mathbb{R}^d$ to output $y \in \mathcal{Y}$, where $\mathcal{Y} = \{1, \dots, K\}$ is the discrete set of K classes. Additionally, we introduce a *soft* version $F : \mathbb{R}^d \rightarrow \mathbb{P}(\mathcal{Y})$ of f , where $\mathbb{P}(\mathcal{Y})$ is the set of probability distributions over \mathcal{Y} . Thus, a soft classifier assigns each data point a distribution over classes, rather than just assigning it to a class. This distribution indicates the likelihood that each class will occur. It is possible to convert any soft classifier F into a hard classifier f by mapping $f(x) = \arg \max_{y \in \mathcal{Y}} F(x)_y$. Additionally, we define as $\mathcal{N}(0, 1)$ the standard Gaussian distribution, as $\Phi(x)$ the Gaussian CDF and as $\Phi^{-1}(x)$ its inverse (or quantile).

Robustness Certificates. Even though an adversarially-trained network is resilient to attacks created during training, it can still be susceptible to unseen new attacks. To overcome this problem, certified defenses formally guarantee the stability of the prediction in a neighbourhood of the input. In other words, a neural network f is certifiably robust for the input $x \in \mathbb{R}^d$, if the prediction for all perturbed versions \tilde{x} remains unchanged such that $\|\tilde{x} - x\|_p \leq \epsilon$, where $\|\cdot\|_p$ is the ℓ_p -norm around x of size $\epsilon > 0$.

Randomized Smoothing. This robustness verification method (Cohen et al., 2019; Lecuyer et al., 2019) computes the ℓ_2 -norm certificates around an input sample x by counting which class is most likely to be returned when x is perturbed by isotropic Gaussian noise. Formally, given a *soft* classifier F , randomized smoothing considers a *smooth* version of F defined as:

$$G(x) \stackrel{\text{def}}{=} \mathbb{E}_{\delta \sim \mathcal{N}(0, \sigma^2 I)} [F(x + \delta)], \quad (1)$$

where $\sigma > 0$ represents the standard deviation. As previously, we define the hard version of $G(x)$ as $g(x) =$

$\arg \max_{y \in \mathcal{Y}} G(x)_y$. Contrary to other formal verification methods, randomized smoothing does not make any assumptions regarding the model’s properties, allowing certification to be scaled to larger and more complex networks. Cohen et al. (2019) demonstrated that G is robust to perturbations of radius R , where the radius R is defined as the difference in probabilities between the most likely class and the second most likely class. A more general interpretation is given by Yang et al. (2020).

Lemma 3.1. [Yang et al. (2020)] *Given a smoothed classifier G defined as in Equation 1, such that $G(x) = (G(x)_1, \dots, G(x)_K)$ is a vector of probabilities that G assigns to each class $1, \dots, K$. Suppose G predicts class c on input x , and the probability is $p = \max_{y \in \mathcal{Y}} G(x)_y > 1/2$, then G continues to predict class c when x is perturbed by any δ with:*

$$\|\delta\|_2 < \sigma \Phi^{-1}(p).$$

One should consider p as the probability that the smoothed classifier will assign to the predicted class rather than any other. As a consequence, if $p > 1/2$, it will continue to do so even if the input is perturbed by Gaussian noise of magnitude smaller than the radius $R = \sigma \Phi^{-1}(p)$. We observe that as p approaches 1, the radius becomes infinite. This makes sense as it only occurs when the original classifier always classify as c .

L -Lipschitz Continuity. Previous works have attempted to convert the robustness analysis problem into a local or global Lipschitz constant estimation problem (Weng et al., 2018; Virmaux & Scaman, 2018; Fazlyab et al., 2019). However, instead of trying to make neural networks Lipschitz continuous, which is difficult while maintaining high accuracy, Salman et al. (2019) show that randomized smoothing can postprocess the network to make it locally Lipschitz continuous. So, let us recall the definition of a L -Lipschitz continuous function.

Definition 3.2 (L -Lipschitz continuous). A function $h : \mathbb{R}^d \rightarrow \mathbb{R}$ is L -Lipschitz continuous in a norm $\|\cdot\|$ if there exists a constant L such that:

$$\forall \tilde{x}, x \in \mathbb{R}^d, \quad |h(\tilde{x}) - h(x)| \leq L \|\tilde{x} - x\|.$$

If h is differentiable, then h is L -Lipschitz continuous if $\|\nabla h(x)\|_* \leq L$ for all x , where $\|\cdot\|_*$ is the dual norm to $\|\cdot\|$. The connection between randomized smoothing and Lipschitz continuity is provided in the following lemma, which offers an analytical form of the gradient of a smooth function.

Lemma 3.3. [Stein (1981)] *Let $\sigma > 0$, let $h : \mathbb{R}^d \rightarrow \mathbb{R}$ be measurable, and let $H(x) = \mathbb{E}_{\delta \sim \mathcal{N}(0, \sigma^2 I)} [h(x + \delta)]$. Then H is differentiable, and moreover:*

$$\nabla H(x) = \frac{1}{\sigma^2} \mathbb{E}_{\delta \sim \mathcal{N}(0, \sigma^2 I)} [\delta \cdot h(x + \delta)].$$

The smoothed function H is also known as the *Weierstrass transform* of h , and a classical property of the Weierstrass transform is its induced smoothness.

Diffusion Denoised Smoothing. A number of recent developments in denoising diffusion probabilistic models have led to state-of-the-art results in image generation (Sohl-Dickstein et al., 2015; Ho et al., 2020; Nichol & Dhariwal, 2021). In a nutshell, forward diffusion involves adding Gaussian noise to an image until it produces an isotropic Gaussian distribution with a large variance. Denoising diffusion probabilistic models work by learning how to reverse this process. In formal terms, given an input sample $x \in \mathbb{R}^d$, a diffusion model selects a predetermined *timestep* $t \in \mathbb{N}^+$ and samples a noisy image x_t as follows:

$$x_t \stackrel{\text{def}}{=} \sqrt{\alpha_t} \cdot x + \sqrt{1 - \alpha_t} \cdot \mathcal{N}(0, I), \quad (2)$$

where the amount of noise to be added to the image is determined by a constant called α_t derived from t .

As Salman et al. (2020) suggested, denoising Gaussian perturbed images leads to out-of-the-box certified robustness for plain models. Following this trend Carlini et al. (2023) make use of a diffusion model as one-shot denoiser achieving state-of-the-art performances. The minor proposed adjustment held in the estimation of t , computed such that $\frac{1 - \alpha_t}{\alpha_t} = \sigma^2$. Additionally, the perturbed version $\tilde{x} = x + \delta$ is scaled by $\sqrt{\alpha_t}$, to match the noise model of Equation 2.

4. Certified Robust OOD Detection

This section explains how using local Lipschitz continuity, achieved through smoothing the classifier with Gaussian noise, can guarantee the detection of OOD samples within a ℓ_2 -sphere around the input.

Preliminaries. To determine how well a classifier distinguishes between ID and OOD samples, it is common to threshold the confidence level and to calculate the area under the receiver operating characteristic curve (AUROC or AUC). Formally, let us consider a function¹ $h \in \mathbb{R}^d \rightarrow \mathbb{R}$, the AUC is defined as:

$$\text{AUC}_h(\mathcal{D}_{in}, \mathcal{D}_{out}) = \mathbb{E}_{\substack{x \sim \mathcal{D}_{in}, \\ z \sim \mathcal{D}_{out}}} [\mathbb{1}_{h(x) > h(z)}],$$

where $\mathcal{D}_{in}, \mathcal{D}_{out}$ are ID and OOD data sets, respectively, and $\mathbb{1}$ returns 1 if the argument is true and 0 otherwise. A number of prior works (Meinke & Hein, 2020; Bitterwolf et al., 2020; Chen et al., 2021; Berrada et al., 2021; Meinke et al., 2022) also investigated the worst-case AUC (WCAUC), which is defined as the lowest AUC attainable when every OOD sample is perturbed so that the highest

level of confidence is achieved within a specific threat model. Specifically, the WCAUC is defined as:

$$\text{WCAUC}_h(\mathcal{D}_{in}, \mathcal{D}_{out}) = \mathbb{E}_{\substack{x \sim \mathcal{D}_{in}, \\ z \sim \mathcal{D}_{out}}} \left[\mathbb{1}_{h(x) > \max_{\|\tilde{z} - z\|_p \leq \epsilon} h(\tilde{z})} \right].$$

Due to the intractable nature of the maximization problem, we can compute upper or lower bounds only, i.e. $\underline{h}(z) \leq \max_{\|\tilde{z} - z\|_p \leq \epsilon} h(\tilde{z}) \leq \bar{h}(z)$. The lower bound $\underline{h}(z)$ is typically calculated using projected gradient methods (Carlini & Wagner, 2017; Croce & Hein, 2020) and named Adversarial AUC (AAUC) (upper bound of WCAUC). In the context of ℓ_∞ -norm, the upper bound $\bar{h}(z)$, called Guaranteed AUC (GAUC) (lower bound of WCAUC), is computed using IBP in Bitterwolf et al. (2020) and Meinke et al. (2022).

Here, we propose a method for computing the upper bound of any classifier without the need for special training or modifications. Thus, the main theorem for an ℓ_2 -norm robustly certified upper bound is stated.

Theorem 4.1. *Let $F : \mathbb{R}^d \rightarrow \mathbb{P}(\mathcal{Y})$ be any soft classifier and G be its associated smooth classifier as defined in Equation 1, with $\sigma > 0$. If $p = \max_{y \in \mathcal{Y}} G(x)_y > 1/2$, then, we have that:*

$$\max_{y \in \mathcal{Y}} G(x + \delta)_y \leq \sqrt{\frac{2}{\pi}} \Phi^{-1}(p) + p, \quad (3)$$

for every $\|\delta\|_2 < \sigma \Phi^{-1}(p)$.

Proof is given in Appendix A. In other words, if the smooth classifier assigns the most likely class more than half the time, it is locally Lipschitz continuous in x , and its maximum prediction is bounded within a radius smaller than $R = \sigma \Phi^{-1}(p)$.

Discussion. While this theorem provides some advantages, it is important to note a couple of its limitations. One of the main limitations is that the upper bound of the smooth classifier G only applies to G and not to the original classifier F . As a result, the guarantee only applies to G , and its robustness at a given input point x cannot be precisely evaluated or certified. To overcome this, Monte Carlo algorithms can be used to approximate these evaluations with high probability (Cohen et al., 2019).

Another limitation is that the guarantees provided by this theorem are only probabilistic in practice. Therefore, a hypothesis test (Hung & Fithian, 2019) should be used to avoid making predictions with low confidence. As with randomized smoothing (Cohen et al., 2019), a large number of samples must be generated in order to achieve high levels of confidence in the certification radius. However, generating these samples can be computationally expensive for complex models.

¹e.g. the Maximum Softmax Probability (Hendrycks & Gimpel, 2017), or the Energy function (Liu et al., 2020).

Despite these limitations, the theorem provides a novel way of calculating the upper bound of any classifier, without the need for special training or modification. Additionally, we provide a tighter certificate compared to previous approaches (Bitterwolf et al., 2020; Meinke et al., 2022), as they used IBP. This can be useful for evaluating the certified robustness of a broader category of standard OOD detection methods as well as larger models, where IBP bounds explode in size and make them unusable (Jovanovic et al., 2021).

5. DISTRO: Diffusion denoised Smoothing for Robust OOD detection

In this section, we present our method. Essentially, it combines three techniques: (i) a diffusion denoiser, (ii) a standard OOD detector, and (iii) a certified binary discriminator. Each component of this method is designed to overcome a specific problem of ordinary classifiers, as they are not robust to adversarial attacks, either ID or OOD, and do not detect OOD inputs well.

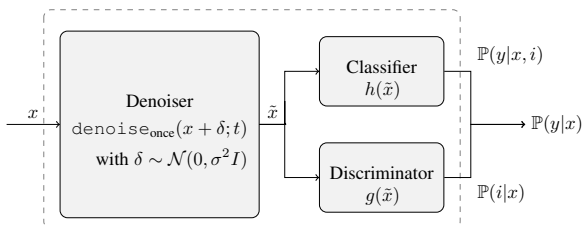


Figure 1: Overview of DISTRO.

In Figure 1, we show an overview of DISTRO. First, a diffusion denoiser is employed before the classifier itself to provide robustness against ID attacks. As a result, adversarial noise introduced by the attack is mitigated by the denoiser. This technique has already been proven to be very efficient and does not affect clean accuracy (Carlini et al., 2023).

Secondly, numerous post-hoc OOD detection methods exist. The most straightforward being MSP (Hendrycks & Gimpel, 2017), which can be added to the image classifier without retraining or fine-tuning. Alternatively, standard OOD detection methods, such as OE (Hendrycks et al., 2019), VOS (Du et al., 2021) or LogitNorm (Wei et al., 2022), could also replace the classifier.

Thirdly, to make the model more robust to OOD adversarial attacks, we add a binary discriminator to the model that is trained to be certifiably robust against OOD attacks. Additionally, this discriminator is combined with the OOD detection method from (ii) which is necessary to have the property of asymptotic underconfidence for far-OOD inputs.

Configuration. This method does not require any new

technical knowledge. We begin by making the assumption that OOD samples are unrelated and thus maximally un-informative to the ID data. Thus, for every class $y \in \mathcal{Y}$, the conditional distribution on the input x is given as:

$$\mathbb{P}(y|x) = \mathbb{P}(y|x, i)\mathbb{P}(i|x) + \frac{1}{K}(1 - \mathbb{P}(i|x)), \quad (4)$$

where $\mathbb{P}(i|x)$ is the conditional distribution representing the probability that x is part of the ID, while $\mathbb{P}(y|x, i)$ is the conditional distribution representing the ID. Similarly to Meinke et al. (2022), we assign independent models to each distribution:

- $\mathbb{P}(y|x, i) = h(\text{denoise}_{\text{once}}(x + \delta; t))$, where $h : \mathbb{R}^d \rightarrow [0, 1]$ is the confidence of the main classifier $F(x)$, and $\tilde{x} = \text{denoise}_{\text{once}}(x + \delta; t)$ represents one single step of denoising operation with $\delta \sim \mathcal{N}(0, \sigma^2 I)$.
- $\mathbb{P}(i|x) = \frac{1}{1 + e^{-g(x)}}$, where $g : \mathbb{R}^d \rightarrow \mathbb{R}$ refers to a binary discriminator trained in a certified robust manner based on an ℓ_∞ -threat model as in Bitterwolf et al. (2020); Meinke et al. (2022).

As can be seen, the denoiser is the main addition. The one-step denoiser $\text{denoise}_{\text{once}}$ estimates the fully denoised image x from the current timestep t . Then it computes the average between the denoised image and the noisy image from the previous timestep. As discussed in Carlini et al. (2023), multiple applications of the denoiser will only destroy information about x . Denoising with iterative steps essentially transfers the classification task to the denoiser, which can determine how the image should be filled. For these reason, we apply only a single step of denoising.

Asymptotic Underconfidence. Here, we show that by coupling a classifier trained to be OOD aware with a diffusion denoiser and running a certified discriminator in parallel, we can guarantee asymptotic underconfidence for data *far enough* from the training distribution.

To obtain asymptotic underconfidence of the joint classifier, we consider $\mathbb{P}(y|x, i) \leq 1$ and rewrite Equation 4 as follows:

$$\mathbb{P}(y|x) \leq \frac{K-1}{K}\mathbb{P}(i|x) + \frac{1}{K}. \quad (5)$$

Since the right term only depends on $\mathbb{P}(i|x)$, we just need to assure that $\lim_{\beta \rightarrow \infty} \mathbb{P}(i|\beta x) \rightarrow 0$. If we employ a certified binary discriminator, trained with IBP on OOD data, as described in Meinke et al. (2022), to compute $\mathbb{P}(i|x)$, we achieve asymptotic underconfidence independently of the main classifier. Readers are referred to Meinke et al. (2022) for a more detailed explanation.

Empirical Evaluation. In Figure 2, we show an empirical evaluation of the asymptotic confidence for standard and

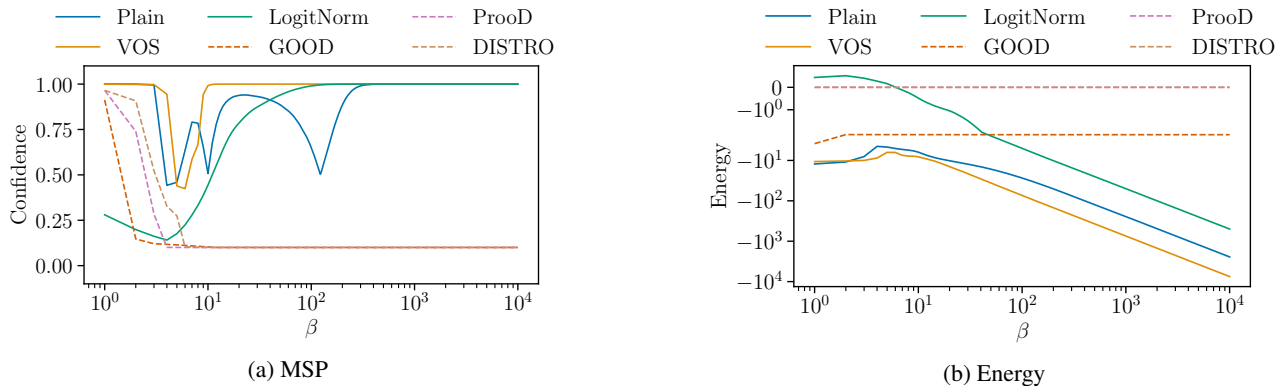


Figure 2: Asymptotic confidence as: (a) MSP (Hendrycks & Gimpel, 2017) and (b) Energy (Liu et al., 2020), for several OOD detection models divided into two categories: *standard* (continuous line) and *guaranteed* (dashed line).

robust OOD detection methods². In this test, we consider a single ID sample x and multiply by a scalar β . In Figure 2a we plot the MSP (Hendrycks & Gimpel, 2017) as confidence, while in Figure 2b we plot the Energy (Liu et al., 2020) for increasing values of $\beta > 0$. In the context of MSP, we observe that standard OOD detection methods are asymptotically overconfident, after a small drop, whereas certified methods such as GOOD (Bitterwolf et al., 2020), ProoD (Meinke et al., 2022) and DISTRO converge to $1/K$. On the other hand, for Energy as β increases, VOS (Du et al., 2021), LogitNorm (Wei et al., 2022), and Plain models asymptotically decrease, whereas GOOD (Bitterwolf et al., 2020), ProoD (Meinke et al., 2022), and DISTRO remain stable.

As a result, underconfidence can be easily obtained when using an energy score instead of MSP, regardless of whether it is on a plain or OOD aware model. However, asymptotic underconfidence does not necessarily imply that the model will perform better in detecting OOD samples since all inputs are usually normalized to some range (e.g. $[0, 1]$ or $[-1, 1]$). Thus the choice of MSP over the energy function is directly related to the possibility of certified robustness for OOD samples.

6. Experiments

In this section, DISTRO is evaluated for a variety of robust ID and OOD tests and is compared to previous approaches.

6.1. Baselines & Settings

As baseline, we consider the pre-trained models³ from Meinke et al. (2022). The normal trained (Plain) and outlier exposure (OE) (Hendrycks et al., 2019) models share the same ResNet18 (He et al., 2016) architecture

and hyperparameters as ProoD (Meinke et al., 2022). GOOD (Bitterwolf et al., 2020) uses a 'XL' convolutional neural network. Additionally, we evaluate the pretrained DenseNet101 (Huang et al., 2017) models for ATOM (Chen et al., 2021) and ACET (Hein et al., 2019); and the standard OOD detection methods: VOS⁴ (Du et al., 2021) and LogitNorm⁵ (Wei et al., 2022) with the pretrained WideResNet40 (Zagoruyko & Komodakis, 2016) models provided in the respective works. We consider DDS (Carlini et al., 2023) with a pre-trained diffusion model⁶ from Nichol & Dhariwal (2021) in front of the OE classifier. With DISTRO, we incorporate the same pre-trained diffusion model of DDS before the main classifier of ProoD, and maintain its discriminator. The diffusion models have been used with the settings described in Carlini et al. (2023). In the context of ℓ_∞ , we set $\sigma = \sqrt{d} \cdot \epsilon$. A list of datasets and additional settings can be found in Appendix B.

6.2. In-Distribution Results

Here, we compare clean, adversarial, and certified accuracy for ID samples. Adversarial accuracy is evaluated with AutoAttack (Croce & Hein, 2020) for ℓ_∞ -norm attacks of budget $\epsilon \in \{2/255, 8/255\}$. We ran the standard version of AutoAttack without additional hyper-parameters. Certified accuracy is evaluated for ℓ_2 -norm robustness of deviation $\sigma \in \{0.12, 0.25\}$. To this end, random smoothing is performed on 10'000 Gaussian distributed samples around the input with a failure probability of 0.001. All $R > 0$ are considered for the certified accuracy. Similarly to Meinke et al. (2022), we adopted the policy of graying out the models with an accuracy drop greater than 3% relative to the model with the highest accuracy. In the context of DISTRO and DDS we run 100 evaluation of the entire test set of CIFAR10 to estimate the clean accuracy and report the

²the models are described in section 6.

³<https://github.com/AlexMeinke/Provable-OOD-Detection>

⁴<https://github.com/deeplearning-wisc/vos>

⁵https://github.com/hongxin001/logitnorm_ood

⁶<https://github.com/openai/improved-diffusion>

average. Further, we ran AutoAttack in both *rand* and *standard* modes, and considered the lowest results for DISTRO and DDS.

Table 2: **ID Accuracy:** Results of clean, adversarial and certified accuracy (%) on the CIFAR10 test set. The grayed-out models have an accuracy drop greater than 3% relative to the model with the highest accuracy.

Method	Clean	Adversarial (ℓ_∞)		Certified (ℓ_2)	
		$\epsilon = 2/255$	$\epsilon = 8/255$	$\sigma = 0.12$	$\sigma = 0.25$
Plain*	95.01	2.16	0.00	28.14	14.17
OE*	95.53	1.97	0.00	31.48	10.88
VOS [†]	94.62	2.24	0.00	13.13	10.02
LogitNorm [‡]	94.48	2.65	0.00	12.53	10.25
ATOM*	92.33	0.00	0.00	0.00	0.00
ACET*	91.49	69.01	6.04	57.13	12.48
GOOD ₈₀ *	90.13	11.65	0.23	17.33	10.31
ProoD* $\Delta = 3$	95.46	2.69	0.00	33.92	13.50
DDS	95.55	72.97	24.09	82.26	64.58
DISTRO (our)	95.47	73.34	27.14	82.77	65.63

* Pre-trained models from Meinke et al. (2022), [†] Pre-trained from Du et al. (2021), [‡] Pre-trained from Wei et al. (2022).

In Table 2, we show the results. As expected, Plain and OE are not robust to adversarial attacks. This applies to ProoD as well, since OE is its primary classifier. Similarly, standard OOD detection methods, as LogitNorm and VOS, show poor robustness for ID data. GOOD demonstrates better results than ProoD for adversarial attacks and worse in terms of certified accuracy. Surprisingly, ACET reveals strong adversarial and certified accuracy despite of its reduced clean accuracy. Meanwhile, ATOM results in zero for all tests since any slight perturbation of the input triggers the last neuron used for OOD detection.

Discussion. It is clear that diffusion models can enhance adversarial and certified robustness while maintaining high clean accuracy. As diffusion introduces variance into gradient estimators, standard attacks become much less effective. Nevertheless, robustness accuracy of diffusion models varies over different runs for the same input, so it should be defined differently from deterministic accuracy, e.g. as expectation. Luckily, one-shot diffusion introduces such a tiny variance that throughout a few of runs, our results were similar.

6.3. Evaluation Metrics

To discriminate between ID and OOD samples, we use the confidence of the classifier, i.e. MSP (Hendrycks & Gimpel, 2017). Traditionally, the following metrics are used to evaluate the OOD detection performance: (i) false positive rate (FPR95) of OODs when ID samples have a 95% true positive rate; (ii) the area under the receiver operating characteristic curve (AUROC or AUC); and (iii) the area under the precision-call curve (AUPR). In order to determine robustness, we compare adversarial (AAUC, AAUPR, AFPR) and guaranteed (GAUC, GAUPR, GFPR) versions of the

previous metrics. In Appendix C, we describe the settings for AAUC, AAUPR and AFPR.

Guaranteed. The guaranteed metrics (GAUC, GAUPR and GFPR) are computed for ℓ_2 and ℓ_∞ norms robustness certificates. Similarly to Meinke et al. (2022), the ℓ_∞ -norm is obtained with IBP⁷ only on OOD data. On the other hand, the ℓ_2 -norm is computed with Theorem 4.1 on both ID and OOD data. Similarly to subsection 6.2, we sampled 10'000 Gaussian data points around the input with a deviation $\sigma = 0.12$. Since, the certified bound is only probabilistic in practice, we ran a binomial proportion confidence test (Brown et al., 2001) with failure probability of 0.001. We have assigned a score of 0 to all samples that fail to be certified, i.e. with $p \leq 1/2$. The Lipschitz continuity does not hold in the case of non-certified samples, therefore we are unable to bound the score. To ensure a fair comparison, we decided to compute the ℓ_2 -norm GAUC on both ID and OOD datasets.

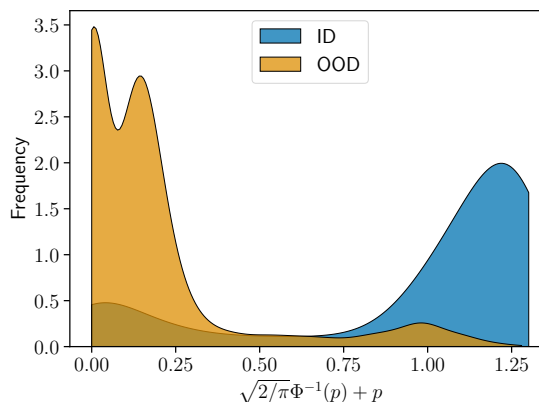


Figure 3: Kernel density estimation (bandwidth = 1) of the distribution of certified smooth ($\sigma = 0.12$) scores for DISTRO on ID (CIFAR10) and OOD (all other datasets) samples.

In Figure 3, we plot the normalized frequency of occurrences of the certified upper bound ($\sqrt{2/\pi} \cdot \Phi^{-1}(p) + p$) for ID versus OOD data of DISTRO. We observe that OOD data tend to peak close to zero, while ID data are spread out with larger values. This suggests that a large radius is more likely to be associated with ID data versus OOD samples. As a result, robustly certifying the detection of OOD samples becomes more feasible.

6.4. Out-Of-Distribution Results

Here, we describe the results shown in Table 3. As previously, we grayed-out models with an accuracy drop greater than 3% with respect to the model with highest accuracy. The objective of this choice is to prioritize clean ID accuracy

⁷For standard OOD detection methods, such as Plain, OE, VOS and LogitNorm, we run IBP-CROWN with auto_LiRPA (Xu et al., 2020).

Diffusion Denoised Smoothing for Certified and Adversarial Robust Out-Of-Distribution Detection

Table 3: **Robust OOD detection.** We consider the following metrics: clean top-1 accuracy on CIFAR10/100 test sets, clean AUC, guaranteed (GAUC), adversarial AUC (AAUC), clean AUPR, guaranteed AUPR (GAUPR), adversarial AUPR (AAUPR), clean FPR95% (FPR), guaranteed FPR95% (GFPR) and adversarial FPR95% (AFPR). Averaging was performed on a variety of OOD datasets. We consider MSP (Hendrycks & Gimpel, 2017) for all methods and metrics (with temperature $T = 1$). The guaranteed ℓ_2 -norm is computed for $\sigma = 0.12$ for all $R > 0$, while the adversarial and guaranteed ℓ_∞ -norm are computed for $\epsilon = 0.01$. The grayed-out models have an accuracy drop greater than 3% relative to the model with the highest accuracy. **Bold** numbers are superior results.

ID: CIFAR10	Acc.	AUC \uparrow	GAUC \uparrow		AAUC \uparrow	AUPR \uparrow	GAUPR \uparrow		AAUPR \uparrow	FPR \downarrow	GFPR \downarrow		AFPR \downarrow
			ℓ_2	ℓ_∞	ℓ_∞		ℓ_2	ℓ_∞	ℓ_∞		ℓ_2	ℓ_∞	ℓ_∞
- Standard													
Plain*	95.01	94.56	48.86	0.00	24.52	99.42	60.05	0.00	82.30	35.72	100.0	100.0	96.72
OE*	95.53	98.78	46.88	0.00	37.91	99.87	63.08	0.00	84.49	4.71	100.0	100.0	70.26
VOS \dagger	94.62	90.82	30.13	0.00	20.62	99.15	41.62	0.00	81.80	61.66	94.10	100.0	100.0
LogitNorm \ddagger	94.48	96.71	40.73	0.00	39.76	99.64	49.31	0.00	86.47	13.95	100.0	100.0	91.10
- Adversarial													
ACET*	91.48	97.24	60.21	0.00	93.01	99.68	76.22	0.00	99.16	13.82	95.65	100.0	32.15
ATOM*	92.33	98.82	97.15	0.00	44.65	99.86	95.51	0.00	85.74	4.14	5.04	100.0	62.65
- Guaranteed													
GOOD $_{s_0}$	90.13	93.12	36.45	57.52	78.11	99.22	52.31	89.54	95.19	30.00	100.0	72.45	47.55
ProoD* $\Delta = 3$	95.46	98.72	52.36	59.56	64.22	99.87	66.53	93.89	94.52	5.49	100.0	100.0	86.49
DISTRO (our)	95.47	98.72	88.97	59.53	83.24	99.87	92.75	93.89	97.32	5.29	67.86	100.0	34.56

ID: CIFAR100	Acc.	AUC \uparrow	GAUC \uparrow		AAUC \uparrow	AUPR \uparrow	GAUPR \uparrow		AAUPR \uparrow	FPR \downarrow	GFPR \downarrow		AFPR \downarrow
			ℓ_2	ℓ_∞	ℓ_∞		ℓ_2	ℓ_∞	ℓ_∞		ℓ_2	ℓ_∞	ℓ_∞
- Standard													
Plain*	77.38	81.60	30.63	0.00	16.98	97.84	45.10	0.00	81.27	82.52	100.0	100.0	100.0
OE*	77.28	90.41	39.87	0.00	22.79	98.90	49.46	0.00	81.96	47.49	100.0	100.0	87.74
- Adversarial													
ACET*	74.47	90.27	36.36	0.00	27.68	98.84	43.50	0.00	82.60	44.11	90.41	100.0	74.99
ATOM*	71.73	91.72	84.38	0.00	31.52	98.88	79.95	0.00	83.36	30.81	30.09	100.0	73.69
- Guaranteed													
ProoD* $\Delta = 1$	76.79	90.90	42.83	37.67	43.81	98.91	50.90	89.66	90.46	42.12	100.0	100.0	97.11
DISTRO (our)	76.78	90.89	59.39	37.53	62.77	98.90	69.41	89.63	93.59	40.94	100.0	100.0	58.58

* Pre-trained models from Meinke et al. (2022), \dagger Pre-trained from Du et al. (2021), \ddagger Pre-trained from Wei et al. (2022).

over all other metrics. A comparison of the remaining metrics is then made on an equal basis. Despite this, there is no direct comparison between the GAUC of ℓ_2 and ℓ_∞ norms. This is primarily due to the fact that the guaranteed upper bound of ℓ_∞ is computed only for OOD data, whereas ℓ_2 is computed for both (ID & OOD). Additionally, we choose any radius $R > 0$ for ℓ_2 , while for ℓ_∞ , ϵ is fixed to 0.01^8 .

We observe that the performances of LogitNorm and VOS on clean AUC, AUPR and FPR are suboptimal. The reason for this is that we are evaluating MSP (Hendrycks & Gimpel, 2017) instead of the suggested normalization (Wei et al., 2022) and energy (Du et al., 2021) functions for LogitNorm and VOS, respectively. To ensure a fair comparison we decided to standardize the output function across all models. On CIFAR100, only the most effective methods of CIFAR10 have been tested.

Outcomes. In light of these considerations, we note that OE achieved the highest clean AUC, AUPR, and FPR. In case of AAUC, ACET shows the best results for CIFAR10. While ATOM achieves close to optimal performance for the

guaranteed ℓ_2 -norm AUC, AUPR and FPR. Both methods are trained adversarially on outliers, which makes them more robust on OOD data, but at the expense of a reduced clean accuracy.

Table 4: Overall average between the metrics of Table 3 for CIFAR10/100 (C-10, C-100).

Method	Average	
	C-10	C-100
Plain	44.02	34.48
OE	50.12	40.42
VOS	38.60	-
LogitNorm	46.31	-
ACET	59.64	41.86
ATOM	64.79	54.38
GOOD $_{s_0}$	64.74	-
ProoD $\Delta = 3$	64.09	52.51
DISTRO (our)	77.08	59.95

in conjunction with the denoiser.

In Table 4, we average all the metrics of Table 3 for CIFAR10 (including clean ID accuracy). Surprisingly,

Similarly to the ID results, DISTRO demonstrates the potential benefits of diffusion models to augment the model robustness in terms of ℓ_2 -norm guaranteed and adversarial AUCs. Although there is a slight decrease in ℓ_∞ -norm GAUC, GAUPR and GFPR, which could likely be suppressed by fine tuning the classifier

⁸This problem can be addressed by considering $R \geq \sqrt{d} \cdot \epsilon$.

ATOM shows similar results as ProoD and GOOD. This can be related to the high certification radius obtained for GAUC of ℓ_2 -norm. We report each individual dataset’s results in [Appendix D](#).

Discussion. It is evident that the ℓ_2 -norm GAUC (and GAUPR) diverge from zero when standard OOD detection models are considered. This illustrates the potential of the ℓ_2 -norm to provide certified OOD detection for any method and architecture. Consequently, it facilitates the experimental evaluation of new robust OOD detection algorithms (both adversarial and certified).

As a side note, the one-shot denoiser appears to improve robustness certification metrics while not compromising clean metrics, such as AUC. In some cases, it also appears to be slightly better, even though the denoising process should produce images that are as similar as possible to those considered during training. This is because a single shot of denoising does not compromise the OOD sample or generate an allucinated one. Additionally, one-shot denoising introduces so little variance that in this benchmark, the results were similar across multiple runs.

In [Appendix E](#), an additional comparison on a similar network architecture for all methods is presented.

7. Conclusion

As of now, certifying the robustness of OOD detection requires external binary discriminators or loose certification mechanisms ([Meinke et al., 2022](#)). This work proposes an alternative approach to compute ℓ_2 -norm robustness certificates for OOD data using randomized smoothing ([Cohen et al., 2019](#)). This technique can be used to certify the confidence of any classifier without requiring certified binary discriminators or specific training methods. In comparison with previously proposed ℓ_∞ -norm GAUC, standard approaches for OOD detection show non-zero results for guaranteed ℓ_2 -norm AUC and AUPR. Unfortunately, a large number of samples derived around the input must be propagated through the network, increasing computational costs.

Additionally, we propose a new method as combination of three techniques. First, we use a diffusion denoiser ([Carlini et al., 2023](#)) to remove noise from adversarial attacks before it reaches the classifier. As a result, we were more successful in defending from adversarial attacks on ID and OOD data. Second, we add an OOD detection method like OE to better distinguish between ID and OOD. Lastly, we include a certified binary discriminator ([Bitterwolf et al., 2020](#); [Meinke et al., 2022](#)) to ensure low confidence for samples *far enough* from the training distribution. Combining these methods improved the performances on several OOD robustness detection metrics by an average of $\sim 13\%/5\%$ relative to previous approaches on CIFAR10/100 datasets.

References

- Andriushchenko, M., Croce, F., Flammarion, N., and Hein, M. Square attack: a query-efficient black-box adversarial attack via random search. In *European Conference on Computer Vision*, pp. 484–501. Springer, 2020.
- Berrada, L., Dathathri, S., Dvijotham, K., Stanforth, R., Bunel, R. R., Uesato, J., Goyal, S., and Kumar, M. P. Make sure you’re unsure: A framework for verifying probabilistic specifications. *Advances in Neural Information Processing Systems*, 34:11136–11147, 2021.
- Biggio, B., Corona, I., Maiorca, D., Nelson, B., Šrđić, N., Laskov, P., Giacinto, G., and Roli, F. Evasion attacks against machine learning at test time. In *Joint European conference on machine learning and knowledge discovery in databases*, pp. 387–402. Springer, 2013.
- Bitterwolf, J., Meinke, A., and Hein, M. Certifiably adversarially robust detection of out-of-distribution data. In Larochelle, H., Ranzato, M., Hadsell, R., Balcan, M., and Lin, H. (eds.), *Advances in Neural Information Processing Systems 33: Annual Conference on Neural Information Processing Systems 2020, NeurIPS 2020, December 6-12, 2020, virtual*, 2020.
- Brown, L. D., Cai, T. T., and DasGupta, A. Interval Estimation for a Binomial Proportion. *Statistical Science*, 16(2): 101 – 133, 2001. doi: 10.1214/ss/1009213286.
- Carlini, N. and Wagner, D. Towards evaluating the robustness of neural networks. In *2017 IEEE Symposium on Security and Privacy (SP)*, pp. 39–57, 2017. doi: 10.1109/SP.2017.49.
- Carlini, N., Tramer, F., Zico Kolter, J., et al. (certified!!) adversarial robustness for free! In *Submitted to The Eleventh International Conference on Learning Representations*, 2023. URL <https://openreview.net/forum?id=JLg5aHHv7j>. under review.
- Chen, J., Li, Y., Wu, X., Liang, Y., and Jha, S. Atom: Robustifying out-of-distribution detection using outlier mining. In *Joint European Conference on Machine Learning and Knowledge Discovery in Databases*, pp. 430–445. Springer, 2021.
- Cimpoi, M., Maji, S., Kokkinos, I., Mohamed, S., and Vedaldi, A. Describing textures in the wild. In *Proceedings of the IEEE Conf. on Computer Vision and Pattern Recognition (CVPR)*, 2014.
- Cohen, J., Rosenfeld, E., and Kolter, Z. Certified adversarial robustness via randomized smoothing. In *International Conference on Machine Learning*, pp. 1310–1320. PMLR, 2019.

- Croce, F. and Hein, M. Reliable evaluation of adversarial robustness with an ensemble of diverse parameter-free attacks. In III, H. D. and Singh, A. (eds.), *Proceedings of the 37th International Conference on Machine Learning*, volume 119 of *Proceedings of Machine Learning Research*, pp. 2206–2216. PMLR, 13–18 Jul 2020.
- Du, X., Wang, Z., Cai, M., and Li, Y. Vos: Learning what you don’t know by virtual outlier synthesis. In *International Conference on Learning Representations*, 2021.
- Engstrom, L., Tran, B., Tsipras, D., Schmidt, L., and Madry, A. Exploring the landscape of spatial robustness. In *International conference on machine learning*, pp. 1802–1811. PMLR, 2019.
- Fazlyab, M., Robey, A., Hassani, H., Morari, M., and Pappas, G. Efficient and accurate estimation of lipschitz constants for deep neural networks. *Advances in Neural Information Processing Systems*, 32, 2019.
- Franco, N., Lorenz, J. M., Roscher, K., and Günnemann, S. Understanding reLU network robustness through test set certification performance, 2023.
- Goodfellow, I., Shlens, J., and Szegedy, C. Explaining and harnessing adversarial examples. In *International Conference on Learning Representations*, 2015.
- Gowal, S., Dvijotham, K., Stanforth, R., Bunel, R., Qin, C., Uesato, J., Arandjelovic, R., Mann, T., and Kohli, P. On the effectiveness of interval bound propagation for training verifiably robust models. *arXiv preprint arXiv:1810.12715*, 2018.
- He, K., Zhang, X., Ren, S., and Sun, J. Deep residual learning for image recognition. In *Proceedings of the IEEE conference on computer vision and pattern recognition*, pp. 770–778, 2016.
- Hein, M., Andriushchenko, M., and Bitterwolf, J. Why relu networks yield high-confidence predictions far away from the training data and how to mitigate the problem. In *IEEE Conference on Computer Vision and Pattern Recognition, CVPR 2019, Long Beach, CA, USA, June 16-20, 2019*, pp. 41–50. Computer Vision Foundation / IEEE, 2019. doi: 10.1109/CVPR.2019.00013.
- Hendrycks, D. and Dietterich, T. Benchmarking neural network robustness to common corruptions and perturbations. In *International Conference on Learning Representations*, 2018.
- Hendrycks, D. and Gimpel, K. A baseline for detecting misclassified and out-of-distribution examples in neural networks. In *International Conference on Learning Representations*, 2017.
- Hendrycks, D., Mazeika, M., and Dietterich, T. G. Deep anomaly detection with outlier exposure. In *7th International Conference on Learning Representations, ICLR 2019, New Orleans, LA, USA, May 6-9, 2019*. OpenReview.net, 2019.
- Ho, J., Jain, A., and Abbeel, P. Denoising diffusion probabilistic models. *Advances in Neural Information Processing Systems*, 33:6840–6851, 2020.
- Huang, G., Liu, Z., Van Der Maaten, L., and Weinberger, K. Q. Densely connected convolutional networks. In *Proceedings of the IEEE conference on computer vision and pattern recognition*, pp. 4700–4708, 2017.
- Hung, K. and Fithian, W. Rank verification for exponential families. *The Annals of Statistics*, 47(2):758–782, 2019.
- Jovanovic, N., Balunovic, M., Baader, M., and Vechev, M. T. Certified defenses: Why tighter relaxations may hurt training? *CoRR*, abs/2102.06700, 2021.
- Katz, G., Barrett, C., Dill, D. L., Julian, K., and Kochenderfer, M. J. Reluplex: An efficient smt solver for verifying deep neural networks. In *International conference on computer aided verification*, pp. 97–117. Springer, 2017.
- Krizhevsky, A., Nair, V., and Hinton, G. Cifar-10 and cifar-100 datasets. URL: <https://www.cs.toronto.edu/kriz/cifar.html>, 6(1):1, 2009.
- Kuznetsova, A., Rom, H., Alldrin, N., Uijlings, J., Krasin, I., Pont-Tuset, J., Kamali, S., Popov, S., Mallocci, M., Kolesnikov, A., et al. The open images dataset v4: Unified image classification, object detection, and visual relationship detection at scale. *International Journal of Computer Vision*, 128(7):1956–1981, 2020.
- Le, Y. and Yang, X. Tiny imagenet visual recognition challenge. *CS 231N*, 7(7):3, 2015.
- Lecuyer, M., Atlidakis, V., Geambasu, R., Hsu, D., and Jana, S. Certified robustness to adversarial examples with differential privacy. In *2019 IEEE Symposium on Security and Privacy (SP)*, pp. 656–672. IEEE, 2019.
- Liu, W., Wang, X., Owens, J., and Li, Y. Energy-based out-of-distribution detection. *Advances in Neural Information Processing Systems*, 33:21464–21475, 2020.
- Madry, A., Makelov, A., Schmidt, L., Tsipras, D., and Vladu, A. Towards deep learning models resistant to adversarial attacks. In *International Conference on Learning Representations*, 2018.
- Meinke, A. and Hein, M. Towards neural networks that provably know when they don’t know. In *8th International Conference on Learning Representations, ICLR 2020, Addis Ababa, Ethiopia, April 26-30, 2020*. OpenReview.net, 2020.

- Meinke, A., Bitterwolf, J., and Hein, M. Provably robust detection of out-of-distribution data (almost) for free. In *NeurIPS*, 2022.
- Mirman, M., Gehr, T., and Vechev, M. Differentiable abstract interpretation for provably robust neural networks. In *International Conference on Machine Learning*, pp. 3578–3586. PMLR, 2018.
- Nichol, A. Q. and Dhariwal, P. Improved denoising diffusion probabilistic models. In *International Conference on Machine Learning*, pp. 8162–8171. PMLR, 2021.
- Paley, A., Urma, R.-G., and Lawrence, N. D. Challenges in deploying machine learning: a survey of case studies. *ACM Computing Surveys*, 55(6):1–29, 2022.
- Salman, H., Li, J., Razenshteyn, I., Zhang, P., Zhang, H., Bubeck, S., and Yang, G. Provably robust deep learning via adversarially trained smoothed classifiers. In Wallach, H., Larochelle, H., Beygelzimer, A., d'Alché-Buc, F., Fox, E., and Garnett, R. (eds.), *Advances in Neural Information Processing Systems*, volume 32. Curran Associates, Inc., 2019.
- Salman, H., Sun, M., Yang, G., Kapoor, A., and Kolter, J. Z. Denoised smoothing: A provable defense for pretrained classifiers. *Advances in Neural Information Processing Systems*, 33:21945–21957, 2020.
- Sermanet, P., Chintala, S., and LeCun, Y. Convolutional neural networks applied to house numbers digit classification. In *Proceedings of the 21st international conference on pattern recognition (ICPR2012)*, pp. 3288–3291, 2012.
- Sohl-Dickstein, J., Weiss, E., Maheswaranathan, N., and Ganguli, S. Deep unsupervised learning using nonequilibrium thermodynamics. In *International Conference on Machine Learning*, pp. 2256–2265. PMLR, 2015.
- Stein, C. M. Estimation of the mean of a multivariate normal distribution. *The annals of Statistics*, pp. 1135–1151, 1981.
- Szegedy, C., Zaremba, W., Sutskever, I., Bruna, J., Erhan, D., Goodfellow, I. J., and Fergus, R. Intriguing properties of neural networks. In Bengio, Y. and LeCun, Y. (eds.), *2nd International Conference on Learning Representations, ICLR 2014, Banff, AB, Canada, April 14-16, 2014, Conference Track Proceedings*, 2014.
- Torralba, A., Fergus, R., and Freeman, W. T. 80 million tiny images: A large data set for nonparametric object and scene recognition. *IEEE transactions on pattern analysis and machine intelligence*, 30(11):1958–1970, 2008.
- Virmaux, A. and Scaman, K. Lipschitz regularity of deep neural networks: analysis and efficient estimation. *Advances in Neural Information Processing Systems*, 31, 2018.
- Wei, H., Xie, R., Cheng, H., Feng, L., An, B., and Li, Y. Mitigating neural network overconfidence with logit normalization. In Chaudhuri, K., Jegelka, S., Song, L., Szepesvari, C., Niu, G., and Sabato, S. (eds.), *Proceedings of the 39th International Conference on Machine Learning*, volume 162 of *Proceedings of Machine Learning Research*, pp. 23631–23644. PMLR, 17–23 Jul 2022.
- Weng, T. W., Zhang, H., Chen, P.-Y., Yi, J., Su, D., Gao, Y., Hsieh, C.-J., and Daniel, L. Evaluating the robustness of neural networks: An extreme value theory approach. In *International Conference on Learning Representations*. International Conference on Learning Representations, ICLR, 2018.
- Wong, E. and Kolter, Z. Provable defenses against adversarial examples via the convex outer adversarial polytope. In Dy, J. and Krause, A. (eds.), *Proceedings of the 35th International Conference on Machine Learning*, volume 80 of *Proceedings of Machine Learning Research*, pp. 5286–5295. PMLR, 10–15 Jul 2018.
- Xu, K., Shi, Z., Zhang, H., Wang, Y., Chang, K.-W., Huang, M., Kaikhura, B., Lin, X., and Hsieh, C.-J. Automatic perturbation analysis for scalable certified robustness and beyond. *Advances in Neural Information Processing Systems*, 33:1129–1141, 2020.
- Yang, G., Duan, T., Hu, J. E., Salman, H., Razenshteyn, I., and Li, J. Randomized smoothing of all shapes and sizes. In *International Conference on Machine Learning*, pp. 10693–10705. PMLR, 2020.
- Yang, J., Wang, P., Zou, D., Zhou, Z., Ding, K., PENG, W., Wang, H., Chen, G., Li, B., Sun, Y., Du, X., Zhou, K., Zhang, W., Hendrycks, D., Li, Y., and Liu, Z. OpenOOD: Benchmarking generalized out-of-distribution detection. In *Thirty-sixth Conference on Neural Information Processing Systems Datasets and Benchmarks Track*, 2022.
- Yu, F., Seff, A., Zhang, Y., Song, S., Funkhouser, T., and Xiao, J. Lsun: Construction of a large-scale image dataset using deep learning with humans in the loop. *arXiv preprint arXiv:1506.03365*, 2015.
- Zagoruyko, S. and Komodakis, N. Wide residual networks. In *British Machine Vision Conference 2016*. British Machine Vision Association, 2016.
- Zhang, H., Weng, T.-W., Chen, P.-Y., Hsieh, C.-J., and Daniel, L. Efficient neural network robustness certification with general activation functions. *Advances in neural information processing systems*, 31, 2018.

A. Proof of Theorem 4.1

Theorem 4.1. Let $F : \mathbb{R}^d \rightarrow \mathbb{P}(\mathcal{Y})$ be any soft classifier and G be its associated smooth classifier as defined in Equation 1, with $\sigma > 0$. If $p = \max_{y \in \mathcal{Y}} G(x)_y > 1/2$, then, we have that:

$$\max_{y \in \mathcal{Y}} G(x + \delta)_y \leq \sqrt{\frac{2}{\pi}} \Phi^{-1}(p) + p, \quad (3)$$

for every $\|\delta\|_2 < \sigma \Phi^{-1}(p)$.

Proof. As a prerequisite to proving the theorem, we need to know the analytic form of the gradient of a smoothed function given in Lemma 3.3. Let us consider the soft classifier $F(x) : \mathbb{R}^d \rightarrow \mathbb{P}(\mathcal{Y})$, and a measurable function $h(x) \stackrel{\text{def}}{=} F(x)_y$, where $y \in \mathcal{Y}$. We define the smooth version of h as $H(x) = \mathbb{E}_{\delta \sim \mathcal{N}(0, \sigma^2 I)} [h(x + \delta)]$, with $\sigma > 0$. Additionally, we consider the Weierstrass transform of h (which coincide with the smooth version of h):

$$H(x) = (h * \mathcal{N}(0, \sigma^2 I))(x) = \mathbb{E}_{\delta \sim \mathcal{N}(0, \sigma^2 I)} [h(x + \delta)],$$

where $*$ denotes the convolution operator. Thus, $H(x)$ is differentiable and:

$$\nabla H(x) = \frac{1}{\sigma^2} \mathbb{E}_{\delta \sim \mathcal{N}(0, \sigma^2 I)} [\delta \cdot h(x + \delta)].$$

Since $h : \mathbb{R}^d \rightarrow [0, 1]$ and ℓ_2 is self-dual, it is sufficient to show that the gradients of H are bounded in ℓ_2 . From Lemma 3.3, for any unit vector $v \in \mathbb{R}^d$ we have:

$$\begin{aligned} |\langle v, \nabla H(x) \rangle| &= \left| \frac{1}{(2\pi\sigma^2)^{d/2}} \int_{\mathbb{R}^d} h(t) \left\langle v, \frac{t-x}{\sigma^2} \right\rangle \exp\left(-\frac{1}{2\sigma^2} \|x-t\|_2^2\right) dt \right|, \\ &\leq \frac{1}{(2\pi\sigma^2)^{d/2}} \int_{\mathbb{R}^d} \left| \left\langle v, \frac{t-x}{\sigma^2} \right\rangle \right| \exp\left(-\frac{1}{2\sigma^2} \|x-t\|_2^2\right) dt, \end{aligned}$$

where we make use of the triangle inequality and know that h is bounded by 1. Given that projections of Gaussians are Gaussians and from the classical integration of the Gaussian density, we obtain:

$$|\langle v, \nabla H(x) \rangle| \leq \frac{1}{(2\pi\sigma^2)^{d/2}} \int_{\mathbb{R}^d} \left| \left\langle v, \frac{t-x}{\sigma^2} \right\rangle \right| \exp\left(-\frac{1}{2\sigma^2} \|x-t\|_2^2\right) dt = \frac{1}{\sigma^2} \mathbb{E}_{Z \sim \mathcal{N}(0, \sigma^2)} [Z] = \sqrt{\frac{2}{\pi\sigma^2}},$$

where we consider the supremum over all unit vectors v . Since, we know that $H(x)$ is $\sqrt{\frac{2}{\pi\sigma^2}}$ -Lipschitz in ℓ_2 , it is possible to use the Lipschitz continuity of H to establish some useful properties. First, it is worth noting that the Lipschitz continuity of H does not directly imply that is concave or convex in x . However, it does imply that H is *well-behaved* in the sense that it does not vary too rapidly with x . Given this, it is possible to use the Lipschitz constant to bound the difference between $H(x + \delta)$ and $H(x)$ for any value of δ , with $\|\delta\|_2 < \sigma \Phi^{-1}(x)$. Formally:

$$\begin{aligned} |H(x + \delta)| - |H(x)| &\leq |H(x + \delta) - H(x)| \leq \sqrt{\frac{2}{\pi\sigma^2}} \|\delta\|_2, \\ |H(x + \delta)| &\leq \sqrt{\frac{2}{\pi\sigma^2}} \|\delta\|_2 + |H(x)|, \end{aligned}$$

where we make use of the reverse triangle inequality. This means that the difference between $H(x + \delta)$ and $H(x)$ is bounded by a multiple of $\|\delta\|_2$. Since $H(x) : \mathbb{R}^d \rightarrow [0, 1]$, we can assume $|H(x)| = H(x)$, and moreover:

$$\begin{aligned} \mathbb{E}_{\delta \sim \mathcal{N}(0, \sigma^2 I)} [h(x + 2\delta)] &\leq \sqrt{\frac{2}{\pi\sigma^2}} \|\delta\|_2 + \mathbb{E}_{\delta \sim \mathcal{N}(0, \sigma^2 I)} [h(x + \delta)], \\ \mathbb{E}_{\delta \sim \mathcal{N}(0, \sigma^2 I)} [F(x + 2\delta)_y] &\leq \sqrt{\frac{2}{\pi\sigma^2}} \|\delta\|_2 + \mathbb{E}_{\delta \sim \mathcal{N}(0, \sigma^2 I)} [F(x + \delta)_y], \\ G(x + 2\delta)_y &\leq \sqrt{\frac{2}{\pi\sigma^2}} \|\delta\|_2 + G(x + \delta)_y, \\ \max_{y \in \mathcal{Y}} G(z + \delta)_y &\leq \sqrt{\frac{2}{\pi\sigma^2}} \|\delta\|_2 + \max_{y \in \mathcal{Y}} G(z)_y, \end{aligned}$$

where in the last step we make a change of variables $z = x + \delta$. Finally, we can insert the certification radius:

$$\max_{y \in \mathcal{Y}} G(z + \delta)_y \leq \sqrt{\frac{2}{\pi}} \Phi^{-1}(z) + \max_{y \in \mathcal{Y}} G(z)_y.$$

□

B. Training, Datasets & Resources

In the context of DISTRO, we use the pre-trained diffusion model with 50M parameters, trained on CIFAR10 with 1000 steps and the cosine noise schedule (Nichol & Dhariwal, 2021). Meanwhile, we trained the same model from scratch on CIFAR100 for 1000 steps, with a batch size of 128, a learning rate of $3e-4$ and the cosine noise schedule. The pretrained models OE, ATOM, ACET, ProoD and GOOD were trained with 80M Tiny Images (Torralba et al., 2008) as OOD dataset. The 80M Tiny Images dataset has been retracted because of concerns about offensive class labels. However, since previous studies have been conducted using this dataset, we compare our results to theirs.

We evaluate all methods on the standard datasets CIFAR10/100 (Krizhevsky et al., 2009) as ID. For the OOD detection evaluation we consider the following set of datasets: CIFAR100/10, SVHN (Sermanet et al., 2012), LSUN (Yu et al., 2015) cropped (LSUN_CR) and resized (LSUN_RS) to 32×32 , TinyImageNet (Le & Yang, 2015) cropped (TinyImageNet_CR) to 32×32 , Textures (Cimpoi et al., 2014) and synthetic (Gaussian and Uniform) noise distributions. We use a random but fixed subset of 1000 images for all datasets considered as a test for OOD. For ID, we consider the entire dataset. We run all our experiments on a single NVIDIA A100.

C. Adversarial AUC, AUPR and FPR

We use the settings in Meinke et al. (2022) to ensure a fair comparison. Our goal is to maximize the confidence within the ℓ_∞ -norm of adversarial attacks on OOD data. We use an ensemble of projected gradient descent (PGD) (Madry et al., 2018) and 5000 queries with the black-box Square Attack (Andriushchenko et al., 2020). APGD (Croce & Hein, 2020) is used with 500 iterations and 5 random restarts. The attack also includes a 200-step PGD with momentum of 0.9 and backtracking that starts with a step size of 0.1, which is halved if the gradient step does not increase confidence, and is multiplied by 1.1 otherwise.

Since robust OOD models are trained to be *flat* on the out-distribution, disappearing gradients (Carlini & Wagner, 2017) pose a significant challenge for evaluating adversarial metrics (Bitterwolf et al., 2020; Meinke et al., 2022). As a result, a variety of starting points is necessary. In following Meinke et al. (2022), we start PGD from: i) a decontrasted version of the image, i.e. the point that minimizes the ℓ_∞ -distance to the grey image $\{0.5\}^d$ within the threat model, ii) 3 uniform samples drawn from the threat model, and iii) 3 versions of the original image perturbed by Gaussian noise with $\sigma = 10^{-4}$ and then clipped to the threat model. All steps of the attack are clipped to $[0, 1]^d$, and the final score for OOD detection is directly optimized.

D. Additional Results

In Table 5, Table 6 and Table 7 we show the results of clean, guaranteed (ℓ_2 and ℓ_∞) and adversarial AUCs, AUPRs and FPRs for each individual datasets. The guaranteed ℓ_2 -norm is computed for $\sigma = 0.12$, while the adversarial and guaranteed ℓ_∞ -norm are computed for $\epsilon = 0.01$. The grayed-out models have an accuracy drop of $> 3\%$ relative to the model with the highest accuracy. **Bold** numbers are superior results.

Table 5: AUC: Clean top-1 accuracy on CIFAR10 test set, clean AUC, adversarial AUC (AAUC) and guaranteed (GAUC) (larger is better).

ID: CIFAR10	Acc.	CIFAR100			SVHN			LSUN_CR			Gaussian						
		AUC	GAUC	AAUC	AUC	GAUC	AAUC	AUC	GAUC	AAUC	AUC	GAUC	AAUC				
		l_2	l_∞	l_∞	l_2	l_∞	l_∞	l_2	l_∞	l_∞	l_2	l_∞	l_∞				
- Standard																	
Plain*	95.01	89.34	51.94	0.00	0.83	94.62	67.08	0.00	0.21	95.12	51.04	0.00	0.97	98.40	39.37	0.00	89.75
OE*	95.53	96.12	50.39	0.00	14.47	99.23	47.61	0.00	0.59	99.38	50.97	0.00	9.04	99.50	39.12	0.00	98.07
VOS†	94.62	87.32	45.36	0.00	0.55	92.05	22.71	0.00	1.57	93.89	54.84	0.00	1.55	87.87	2.10	0.00	72.01
LogitNorm‡	94.48	91.15	45.06	0.00	7.48	96.52	45.38	0.00	2.49	98.99	44.97	0.00	14.74	97.99	25.74	0.00	94.34
- Adversarial																	
ACET*	91.48	90.64	62.54	0.00	79.52	95.24	62.69	0.00	87.88	98.65	60.90	0.00	95.67	99.93	57.30	0.00	99.93
ATOM*	92.33	93.55	84.22	0.00	14.93	99.58	99.29	0.00	8.14	99.68	99.42	0.00	36.69	99.93	100.0	0.00	99.93
- Guaranteed																	
GOOD ₅₀	90.13	86.25	40.64	42.56	62.86	94.14	48.67	35.31	65.48	94.39	47.34	50.33	77.96	96.02	21.41	95.53	95.94
ProoD* $\Delta = 3$	95.46	95.93	52.29	41.82	43.80	99.44	57.29	47.26	48.03	99.43	55.49	61.72	63.22	99.33	44.26	85.18	95.86
DISTRO (our)	95.47	95.90	87.88	41.79	64.76	99.44	90.95	47.22	74.45	99.42	89.13	61.67	87.75	99.38	87.87	85.22	98.86
ID: CIFAR10	Acc.	LSUN_RS			TinyImageNet_CR			Textures			Uniform						
		AUC	GAUC	AAUC	AUC	GAUC	AAUC	AUC	GAUC	AAUC	AUC	GAUC	AAUC				
		l_2	l_∞	l_∞	l_2	l_∞	l_∞	l_2	l_∞	l_∞	l_2	l_∞	l_∞				
- Standard																	
Plain*	95.01	94.82	51.41	0.00	9.61	94.30	45.87	0.00	6.93	92.09	46.40	0.00	5.16	97.77	37.80	0.00	82.70
OE*	95.53	98.87	53.04	0.00	31.25	98.21	50.51	0.00	21.06	99.40	45.47	0.00	33.93	99.49	37.95	0.00	94.85
VOS†	94.62	93.51	28.51	0.00	9.17	92.48	29.00	0.00	5.42	88.05	53.50	0.00	3.84	91.41	5.05	0.00	70.83
LogitNorm‡	94.48	98.38	41.43	0.00	49.25	98.05	35.13	0.00	38.02	94.28	49.05	0.00	19.46	98.34	39.09	0.00	92.30
- Adversarial																	
ACET*	91.48	98.93	60.14	0.00	96.51	96.50	60.26	0.00	90.77	98.12	60.56	0.00	93.87	99.95	57.30	0.00	99.95
ATOM*	92.33	99.24	99.04	0.00	22.59	99.12	97.43	0.00	22.36	99.55	97.81	0.00	52.62	99.93	100.0	0.00	99.93
- Guaranteed																	
GOOD ₅₀	90.13	91.82	39.77	49.15	75.82	90.77	38.44	48.25	70.63	95.79	39.04	43.75	80.56	95.76	16.30	95.31	95.63
ProoD* $\Delta = 3$	95.46	98.71	55.83	49.64	54.07	98.23	55.54	49.70	52.69	99.40	52.22	60.81	65.34	99.32	46.00	80.42	90.72
DISTRO (our)	95.47	98.70	90.40	49.60	78.54	98.21	89.22	49.66	74.12	99.40	88.58	60.76	89.83	99.31	87.75	80.33	97.61
ID: CIFAR100	Acc.	CIFAR100			SVHN			LSUN_CR			Gaussian						
		AUC	GAUC	AAUC	AUC	GAUC	AAUC	AUC	GAUC	AAUC	AUC	GAUC	AAUC				
		l_2	l_∞	l_∞	l_2	l_∞	l_∞	l_2	l_∞	l_∞	l_2	l_∞	l_∞				
- Standard																	
Plain*	77.38	77.13	57.97	0.00	0.81	83.36	41.32	0.00	2.38	81.96	28.89	0.00	1.48	86.93	20.97	0.00	64.31
OE*	77.28	83.40	52.77	0.00	1.01	93.59	39.79	0.00	1.07	93.05	34.24	0.00	1.87	97.36	53.50	0.00	86.90
- Adversarial																	
ACET*	74.47	79.18	47.73	0.00	0.53	90.60	37.24	0.00	0.29	94.01	27.38	0.00	1.55	99.45	81.64	0.00	98.98
ATOM*	71.73	63.03	53.01	0.00	0.11	93.51	84.66	0.00	0.21	96.56	89.57	0.00	7.41	99.98	100.0	0.00	99.98
- Guaranteed																	
ProoD* $\Delta = 1$	76.79	80.09	54.18	22.21	22.43	94.58	43.77	33.29	33.54	94.35	40.84	34.58	35.00	98.19	46.66	60.41	85.57
DISTRO (our)	76.78	80.15	66.72	22.11	34.14	95.08	65.02	33.15	48.36	94.38	56.51	34.45	59.76	97.78	63.15	60.26	97.51
ID: CIFAR100	Acc.	LSUN_RS			TinyImageNet_CR			Textures			Uniform						
		AUC	GAUC	AAUC	AUC	GAUC	AAUC	AUC	GAUC	AAUC	AUC	GAUC	AAUC				
		l_2	l_∞	l_∞	l_2	l_∞	l_∞	l_2	l_∞	l_∞	l_2	l_∞	l_∞				
- Standard																	
Plain*	77.38	77.56	26.13	0.00	3.58	84.26	25.72	0.00	4.62	77.87	29.02	0.00	3.78	83.72	15.00	0.00	54.90
OE*	77.28	85.86	29.03	0.00	5.56	84.23	32.76	0.00	5.09	90.12	33.32	0.00	9.86	95.68	43.52	0.00	70.97
- Adversarial																	
ACET*	74.47	86.55	9.15	0.00	9.42	83.35	13.90	0.00	7.94	87.46	26.26	0.00	4.60	99.54	47.61	0.00	98.04
ATOM*	71.73	96.58	91.13	0.00	19.13	93.02	82.30	0.00	12.57	91.06	74.40	0.00	12.96	99.98	100.0	0.00	99.98
- Guaranteed																	
ProoD* $\Delta = 1$	76.79	86.21	30.06	33.53	34.48	85.16	38.18	28.54	29.47	91.25	36.96	31.58	33.65	97.41	52.00	57.22	76.33
DISTRO (our)	76.78	86.08	57.01	33.39	57.63	85.07	58.33	28.42	47.64	91.20	54.88	31.45	59.87	97.37	53.50	57.01	97.05

* Pre-trained models from Meinke et al. (2022), † Pre-trained from Du et al. (2021), ‡ Pre-trained from Wei et al. (2022).

Table 6: **AUPR**: Clean top-1 accuracy on CIFAR10 test set, clean AUPR, guaranteed (GAUPR) and adversarial AUPR (AAUPR) (larger is better).

ID: CIFAR10	Acc.	AUPR	CIFAR100			AUPR	SVHN			AUPR	LSUN_CR			AUPR	Gaussian		
			GAUPR	AAUPR	l_∞		GAUPR	AAUPR	l_∞		GAUPR	AAUPR	l_∞		GAUPR	AAUPR	l_∞
			l_2	l_∞	l_∞		l_2	l_∞	l_∞		l_2	l_∞	l_∞		l_2	l_∞	l_∞
- Standard																	
Plain*	95.01	98.76	60.36	0.00	76.18	99.43	72.48	0.00	76.08	99.50	63.13	0.00	76.20	99.83	59.39	0.00	98.96
OE*	95.53	99.57	63.41	0.00	78.46	99.92	64.10	0.00	76.12	99.94	64.37	0.00	77.56	99.95	61.04	0.00	99.79
VOS [†]	94.62	98.42	48.39	0.00	76.17	99.16	37.97	0.00	76.38	99.34	53.75	0.00	76.37	99.34	31.48	0.00	96.85
LogitNorm [‡]	94.48	98.97	51.35	0.00	77.79	96.52	50.49	0.00	76.53	98.99	50.93	0.00	79.48	97.99	42.25	0.00	99.46
- Adversarial																	
ACET*	91.48	98.84	74.80	0.00	97.20	99.49	77.14	0.00	98.66	99.86	76.80	0.00	99.53	99.99	76.09	0.00	99.99
ATOM*	92.33	99.20	76.27	0.00	78.51	99.95	98.74	0.00	77.35	99.96	98.96	0.00	82.65	99.99	100.0	0.00	99.99
- Guaranteed																	
GOOD ₈₀ *	90.13	98.25	51.86	85.62	90.76	99.35	59.85	83.46	91.06	99.39	58.05	87.11	95.40	99.63	46.39	99.59	99.62
Prood* $\Delta = 3$	95.46	99.55	65.46	89.73	90.13	99.94	68.75	91.06	91.27	99.94	67.83	94.46	94.74	99.94	64.20	98.55	99.59
DISTRO (our)	95.47	99.55	90.96	89.73	93.72	99.94	93.84	91.05	95.55	99.94	93.02	94.46	98.21	99.94	87.87	98.55	99.89
ID: CIFAR10	Acc.	AUPR	LSUN_RS			AUPR	TinyImageNet_CR			AUPR	Textures			AUPR	Uniform		
			GAUPR	AAUPR	l_∞		GAUPR	AAUPR	l_∞		GAUPR	AAUPR	l_∞		GAUPR	AAUPR	l_∞
			l_2	l_∞	l_∞		l_2	l_∞	l_∞		l_2	l_∞	l_∞		l_2	l_∞	l_∞
- Standard																	
Plain*	95.01	99.47	59.44	0.00	78.33	99.41	55.39	0.00	77.54	99.14	56.72	0.00	77.00	99.77	60.05	0.00	98.15
OE*	95.53	99.89	64.75	0.00	82.45	99.82	63.29	0.00	80.13	99.94	62.81	0.00	82.06	99.95	60.91	0.00	99.35
VOS [†]	94.62	99.31	39.59	0.00	78.02	99.19	38.37	0.00	77.16	98.35	51.56	0.00	76.81	99.15	31.88	0.00	96.64
LogitNorm [‡]	94.48	99.84	48.63	0.00	91.87	99.80	45.03	0.00	87.05	99.32	54.20	0.00	80.32	99.84	51.60	0.00	99.25
- Adversarial																	
ACET*	91.48	99.89	76.61	0.00	99.62	99.62	75.72	0.00	98.95	99.80	76.47	0.00	99.32	99.99	76.09	0.00	99.99
ATOM*	92.33	99.93	98.56	0.00	81.18	99.91	95.55	0.00	80.49	99.95	95.99	0.00	85.80	99.99	100.0	0.00	99.93
- Guaranteed																	
GOOD ₈₀ *	90.13	99.09	52.78	88.42	96.01	98.95	51.23	87.51	94.12	99.52	53.08	85.03	94.93	99.61	45.27	99.56	99.59
Prood* $\Delta = 3$	95.46	99.87	67.42	92.42	93.26	99.82	66.99	92.41	93.00	99.94	66.76	94.49	95.14	99.94	64.85	98.03	99.07
DISTRO (our)	95.47	99.87	93.10	92.41	96.82	99.82	92.23	92.41	96.14	99.94	92.91	94.48	98.45	99.93	93.01	98.02	99.75
ID: CIFAR100	Acc.	AUPR	CIFAR100			AUPR	SVHN			AUPR	LSUN_CR			AUPR	Gaussian		
			GAUPR	AAUPR	l_∞		GAUPR	AAUPR	l_∞		GAUPR	AAUPR	l_∞		GAUPR	AAUPR	l_∞
			l_2	l_∞	l_∞		l_2	l_∞	l_∞		l_2	l_∞	l_∞		l_2	l_∞	l_∞
- Standard																	
Plain*	77.38	97.08	60.35	0.00	76.16	98.09	48.36	0.00	76.53	97.87	43.69	0.00	76.3	98.68	41.33	0.00	95.95
OE*	77.28	98.06	57.15	0.00	76.18	99.31	51.21	0.00	76.21	99.25	47.99	0.00	76.35	99.71	53.44	0.00	98.44
- Adversarial																	
ACET*	74.47	79.18	47.98	0.00	76.09	90.60	41.95	0.00	76.05	94.01	37.41	0.00	76.30	99.45	72.01	0.00	99.90
ATOM*	71.73	94.36	53.01	0.00	76.04	99.30	77.57	0.00	76.06	99.63	83.44	0.00	77.32	100.0	100.0	0.00	100.0
- Guaranteed																	
Prood* $\Delta = 1$	76.79	97.42	57.84	85.51	85.56	99.43	52.25	89.27	89.34	99.37	51.30	88.10	88.22	99.82	51.41	95.53	98.42
DISTRO (our)	76.78	97.43	70.75	85.48	88.21	99.49	72.41	89.24	92.05	99.37	68.69	88.07	92.62	99.78	72.65	95.51	99.75
ID: CIFAR100	Acc.	AUPR	LSUN_RS			AUPR	TinyImageNet_CR			AUPR	Textures			AUPR	Uniform		
			GAUPR	AAUPR	l_∞		GAUPR	AAUPR	l_∞		GAUPR	AAUPR	l_∞		GAUPR	AAUPR	l_∞
			l_2	l_∞	l_∞		l_2	l_∞	l_∞		l_2	l_∞	l_∞		l_2	l_∞	l_∞
- Standard																	
Plain*	77.38	97.27	42.43	0.00	76.80	98.15	42.44	0.00	77.06	97.26	42.16	0.00	76.80	98.29	40.01	0.00	94.55
OE*	77.28	98.34	46.67	0.00	77.24	98.13	45.90	0.00	77.07	98.83	46.55	0.00	77.91	99.58	48.75	0.00	96.28
- Adversarial																	
ACET*	74.47	86.55	32.77	0.00	78.06	85.35	33.58	0.00	77.68	87.46	36.51	0.00	76.92	99.54	45.81	0.00	99.81
ATOM*	71.73	99.64	85.92	0.00	80.44	99.24	74.55	0.00	78.66	98.87	66.51	0.00	78.41	100.0	100.0	0.00	100.0
- Guaranteed																	
Prood* $\Delta = 1$	76.79	98.35	45.57	89.23	89.47	98.17	47.29	87.20	87.45	98.96	48.27	87.36	87.84	99.74	53.30	95.06	97.36
DISTRO (our)	76.78	98.33	67.15	89.20	93.24	98.16	66.89	87.17	90.80	98.95	67.11	87.33	92.40	99.74	69.60	95.03	99.68

 * Pre-trained models from Meinke et al. (2022), [†] Pre-trained from Du et al. (2021), [‡] Pre-trained from Wei et al. (2022).

Table 7: **FPR@95**: Clean top-1 accuracy on CIFAR10 test set, clean FPR, guaranteed (GFPR) and adversarial FPR (AFPR) (smaller is better).

ID: CIFAR10	Acc.	FPR	CIFAR100			FPR	SVHN			FPR	LSUN_CR			FPR	Gaussian		
			GFPR		AFPR		GFPR		AFPR		GFPR		AFPR		GFPR		AFPR
			ℓ_2	ℓ_∞	ℓ_∞		ℓ_2	ℓ_∞	ℓ_∞		ℓ_2	ℓ_∞	ℓ_∞		ℓ_2	ℓ_∞	ℓ_∞
- Standard																	
Plain	95.01	61.0	100.0	100.0	100.0	37.5	100.0	100.0	100.0	35.4	100.0	100.0	100.0	7.6	100.0	100.0	74.3
OE	95.53	21.3	100.0	100.0	89.8	1.8	100.0	100.0	99.8	1.2	100.0	100.0	94.9	0.8	100.0	100.0	11.6
VOS	94.62	65.1	94.8	100.0	100.0	55.6	98.3	100.0	100.0	39.7	80.6	100.0	100.0	96.2	100.0	100.0	100.0
LogitNorm	94.48	43.9	100.0	100.0	100.0	16.3	100.0	100.0	100.0	4.2	100.0	100.0	99.7	2.4	100.0	100.0	52.5
- Adversarial																	
ACET	91.48	40.4	91.3	100.0	67.4	29.4	93.4	100.0	63.5	5.9	93.4	100.0	24.2	0.0	100.0	100.0	0.0
ATOM	92.33	27.7	29.3	100.0	89.5	0.9	1.1	100.0	94.6	0.6	0.9	100.0	73.1	0.0	0.0	100.0	0.0
- Guaranteed																	
GOOD ₅₀	90.13	51.2	100.0	96.7	70.1	33.5	100.0	99.6	65.1	36.1	100.0	97.1	64.7	0.0	100.0	0.0	0.0
ProoD $\Delta = 3$	95.46	23.7	100.0	100.0	93.9	1.7	100.0	100.0	99.9	1.6	100.0	100.0	96.3	0.2	100.0	100.0	16.5
DISTRO (our)	95.47	23.7	64.4	100.0	59.0	1.6	54.4	100.0	46.8	1.5	68.3	100.0	31.4	0.2	83.7	100.0	5.0
ID: CIFAR10	Acc.	FPR	LSUN_RS			FPR	TinyImageNet_CR			FPR	Textures			FPR	Uniform		
			GFPR		AFPR		GFPR		AFPR		GFPR		AFPR		GFPR		AFPR
			ℓ_2	ℓ_∞	ℓ_∞		ℓ_2	ℓ_∞	ℓ_∞		ℓ_2	ℓ_∞	ℓ_∞		ℓ_2	ℓ_∞	ℓ_∞
- Standard																	
Plain*	95.01	37.9	100.0	100.0	100.0	40.8	100.0	100.0	100.0	52.5	100.0	100.0	100.0	12.5	100.0	100.0	99.5
OE*	95.53	3.1	100.0	100.0	80.6	8.3	100.0	100.0	88.6	1.7	100.0	100.0	73.8	0.0	100.0	100.0	23.0
VOS [†]	94.62	45.4	97.3	100.0	100.0	50.5	95.4	100.0	100.0	59.1	86.5	100.0	100.0	81.7	99.9	100.0	100.0
LogitNorm [‡]	94.48	6.7	100.0	100.0	99.3	9.8	100.0	100.0	98.9	27.5	100.0	100.0	98.6	0.8	100.0	100.0	79.8
- Adversarial																	
ACET*	91.48	5.3	96.1	100.0	20.5	18.6	94.7	100.0	48.1	11.0	95.4	100.0	33.5	0.0	100.0	100.0	0.0
ATOM*	92.33	0.6	1.1	100.0	97.1	1.6	4.1	100.0	92.4	1.5	3.8	100.0	54.5	0.00	0.00	100.0	0.0
- Guaranteed																	
GOOD ₅₀	90.13	49.3	100.0	98.8	65.4	48.7	100.0	96.5	69.3	21.2	100.0	90.3	45.4	0.0	100.0	0.6	0.3
ProoD* $\Delta = 3$	95.46	5.1	100.0	100.0	87.8	8.8	100.0	100.0	92.8	1.4	100.0	100.0	84.8	0.3	100.0	100.0	34.7
DISTRO (our)	95.47	5.0	51.8	100.0	46.4	8.9	58.3	100.0	53.8	1.1	74.8	100.0	23.1	0.3	87.2	100.0	11.0
ID: CIFAR100	Acc.	FPR	CIFAR100			FPR	SVHN			FPR	LSUN_CR			FPR	Gaussian		
			GFPR		AFPR		GFPR		AFPR		GFPR		AFPR		GFPR		AFPR
			ℓ_2	ℓ_∞	ℓ_∞		ℓ_2	ℓ_∞	ℓ_∞		ℓ_2	ℓ_∞	ℓ_∞		ℓ_2	ℓ_∞	ℓ_∞
- Standard																	
Plain*	77.38	80.5	100.0	100.0	100.0	74.0	100.0	100.0	100.0	75.0	100.0	100.0	100.0	97.6	100.0	100.0	100.0
OE*	77.28	73.9	100.0	100.0	100.0	36.6	100.0	100.0	100.0	39.9	100.0	100.0	99.8	13.5	100.0	100.0	39.0
- Adversarial																	
ACET*	74.47	81.8	96.2	100.0	100.0	54.8	97.0	100.0	100.0	32.8	96.8	100.0	100.0	0.0	49.7	100.0	0.0
ATOM*	71.73	89.8	88.9	100.0	100.0	37.1	30.6	100.0	100.0	20.0	19.6	96.9	96.9	0.0	0.0	100.0	0.0
- Guaranteed																	
ProoD* $\Delta = 1$	76.79	79.4	100.0	100.0	100.0	32.1	100.0	100.0	100.0	31.1	100.0	100.0	100.0	4.8	100.0	100.0	77.3
DISTRO (our)	76.78	80.2	100.0	100.0	90.6	29.9	100.0	100.0	85.6	31.2	100.0	100.0	63.8	8.5	100.0	100.0	7.2
ID: CIFAR100	Acc.	FPR	LSUN_RS			FPR	TinyImageNet_CR			FPR	Textures			FPR	Uniform		
			GFPR		AFPR		GFPR		AFPR		GFPR		AFPR		GFPR		AFPR
			ℓ_2	ℓ_∞	ℓ_∞		ℓ_2	ℓ_∞	ℓ_∞		ℓ_2	ℓ_∞	ℓ_∞		ℓ_2	ℓ_∞	ℓ_∞
- Standard																	
Plain	77.38	81.7	100.0	100.0	100.0	69.0	100.0	100.0	100.0	84.0	100.0	100.0	100.0	96.8	100.0	100.0	100.0
OE	77.28	66.0	100.0	100.0	99.5	69.6	100.0	100.0	99.5	48.1	100.0	100.0	96.5	31.6	100.0	100.0	67.8
- Adversarial																	
ACET	74.47	62.7	99.7	100.0	100.0	61.6	99.1	100.0	100.0	59.2	96.9	100.0	100.0	0.0	87.9	100.0	0.0
ATOM	71.73	20.8	17.4	100.0	97.2	39.8	34.2	100.0	98.7	39.0	50.0	100.0	96.7	0.0	0.0	100.0	0.0
- Guaranteed																	
ProoD $\Delta = 1$	76.79	62.0	100.0	100.0	99.9	68.6	100.0	100.0	99.9	45.6	100.0	100.0	99.8	13.4	100.0	100.0	100.0
DISTRO (our)	76.78	62.6	100.0	100.0	71.7	69.0	100.0	100.0	80.3	46.1	100.0	100.0	61.2	11.2	100.0	100.0	8.2

* Pre-trained models from Meinke et al. (2022), † Pre-trained from Du et al. (2021), ‡ Pre-trained from Wei et al. (2022).

E. Experimental Results on Similar Model Capacity

In this section we compare each method on a similar model architecture, since the results in Table 1 are not only dependent on the method performance, but also on the capacity of the model and OOD dataset used. Therefore we retrain all presented methods using a ResNet18 architecture for CIFAR10 and CIFAR100 respectively. For methods that require an additional OOD dataset for training, such as OE (Hendrycks et al., 2019), ACET (Hein et al., 2019), ATOM (Chen et al., 2021), ProoD (Meinke et al., 2022) and DISTRO, we use the same subset of OpenImages (Kuznetsova et al., 2020) containing 50'000 images. Furthermore, we consider an input normalization of 0.5 across all dimensions for both mean and standard deviation. In addition, we attempt to be as minimally intrusive as possible when it comes to the default training procedure.

For Plain, OE and LogitNorm we run the implementation⁹ from Yang et al. (2022) and leave the hyperparameters unchanged. Similarly for ACET and ATOM, we only change the model architecture and normalization and run both implementations from ATOM¹⁰. Lastly, we train ProoD¹¹ from Meinke et al. (2022) using their training configuration files, where the discriminator is trained for 1000 epochs and the bias shift (Δ) is 3/1 for CIFAR10/100, respectively.

Table 8: **Robust OOD detection with ResNet18.** The guaranteed ℓ_2 -norm is computed for $\sigma = 0.12$, while the adversarial and guaranteed ℓ_∞ -norm are computed for $\epsilon = 0.01$. The grayed-out models have an accuracy drop of $> 3\%$ relative to the model with the highest accuracy. **Bold** numbers are superior results.

ID: CIFAR10	Acc.	AUC \uparrow	GAUC \uparrow		AAUC \uparrow	AUPR \uparrow	GAUPR \uparrow		AAUPR \uparrow	FPR \downarrow	GFPR \downarrow		AFPR \downarrow
			ℓ_2	ℓ_∞	ℓ_∞		ℓ_2	ℓ_∞	ℓ_∞		ℓ_2	ℓ_∞	ℓ_∞
Plain	94.32	92.28	35.81	0.00	23.71	99.00	46.83	0.00	82.00	40.21	93.56	100.0	98.88
LogitNorm	94.71	95.58	34.19	0.00	35.00	99.54	49.63	0.00	85.14	33.06	95.12	100.0	92.20
OE	92.41	97.35	50.56	0.00	37.95	99.71	62.25	0.00	85.51	13.44	100.0	100.0	74.91
ACET	93.66	97.86	37.45	0.00	65.21	99.75	50.26	0.00	91.99	8.94	100.0	100.0	50.29
ATOM	91.90	98.12	97.98	97.63	62.79	99.78	98.16	99.78	91.49	8.7	9.42	0.00	51.56
ProoD	95.20	96.91	44.95	63.44	64.61	99.63	60.27	94.37	94.42	16.03	100.0	91.90	78.22
DISTRO (our)	95.20	96.80	86.63	59.86	71.70	99.62	90.80	93.78	95.72	16.55	66.88	99.96	67.59

ID: CIFAR100	Acc.	AUC \uparrow	GAUC \uparrow		AAUC \uparrow	AUPR \uparrow	GAUPR \uparrow		AAUPR \uparrow	FPR \downarrow	GFPR \downarrow		AFPR \downarrow
			ℓ_2	ℓ_∞	ℓ_∞		ℓ_2	ℓ_∞	ℓ_∞		ℓ_2	ℓ_∞	ℓ_∞
Plain	77.54	84.50	38.11	0.00	24.17	98.16	44.96	0.00	82.32	67.61	100.0	100.0	98.04
LogitNorm	76.25	84.06	40.93	0.00	47.64	98.04	46.80	0.00	87.25	73.70	100.0	100.0	87.98
OE	75.84	88.96	38.90	0.00	17.90	98.72	48.82	0.00	81.43	49.61	100.0	100.0	99.41
ACET	73.71	95.65	42.03	0.00	52.49	99.44	48.54	0.00	89.23	13.96	100.0	100.0	60.39
ProoD	77.77	89.47	40.72	37.68	49.16	98.66	49.97	89.66	91.08	40.44	100.0	100.0	84.15
DISTRO (our)	77.73	88.90	55.57	29.71	51.89	98.60	67.62	87.44	91.71	43.24	100.0	100.0	79.34

⁹<https://github.com/Jingkang50/OpenOOD>

¹⁰<https://github.com/jfc43/informative-outlier-mining>

¹¹<https://github.com/AlexMeinke/Provable-OOD-Detection>